Appl Biochem Biotechnol (2007) 143:1–15
DOI 10.1007/s12010-007-0027-2

Mutation of Tyr-218 to Phe in *Thermoanaerobacter ethanolicus* Secondary Alcohol Dehydrogenase: Effects on Bioelectronic Interface Performance

Brian L. Hassler · Megan Dennis · Maris Laivenieks · J. Gregory Zeikus · Robert M. Worden

Received: 31 July 2006 / Revised: 6 November 2006 / Accepted: 24 January 2007 /
Published online: 17 April 2007

Abstract Bioelectronic interfaces that facilitate electron transfer between the electrode and a dehydrogenase enzyme have potential applications in biosensors, biocatalytic reactors, and biological fuel cells. The secondary alcohol dehydrogenase (2° ADH) from *Thermoanaerobacter ethanolicus* is especially well suited for the development of such bioelectronic interfaces because of its thermostability and facile production and purification. However, the natural cofactor for the enzyme, β-nicotinamide adenine dinucleotide phosphate ($NADP^+$), is more expensive and less stable than β-nicotinamide adenine dinucleotide (NAD^+). PCR-based, site-directed mutagenesis was performed on 2° ADH in an attempt to adjust the cofactor specificity toward NAD^+ by mutating Tyr^{218} to Phe (Y218F 2° ADH). This mutation increased the K_m(app) for $NADP^+$ 200-fold while decreasing the K_m(app) for NAD^+ 2.5-fold. The mutant enzyme was incorporated into a bioelectronic interface that established electrical communication between the enzyme, the NAD^+, the electron mediator toluidine blue O (TBO), and a gold electrode. Cyclic voltammetry, impedance spectroscopy, gas chromatography, mass spectrometry, constant potential amperometry, and chronoamperometry were used to characterize the mutant and wild-type enzyme incorporated in the bioelectronic interface. The Y218F 2° ADH exhibited a fourfold increase in the turnover ratio compared to the wild type in the presence of NAD^+. The electrochemical and kinetic measurements support the prediction that the Rossmann fold of the enzyme binds to the phosphate moiety of the cofactor. During the 45 min of continuous operation, NAD^+ was electrically recycled 6.7×10^4 times, suggesting that the Y218F 2° ADH-modified bioelectronic interface is stable.

Keywords Secondary alcohol dehydrogenase · Biosensor · Cofactor regeneration · Site-directed mutagenesis · Bioelectronic · Biocatalysis · Electron mediator · Toluidine blue · $NADP^+$ · NAD^+

B. L. Hassler · M. Dennis · R. M. Worden (✉)
Department of Chemical Engineering and Materials Science, Michigan State University,
East Lansing, MI 48824, USA
e-mail: worden@egr.msu.edu

M. Laivenieks · J. G. Zeikus
Department of Biochemistry and Molecular Biology, Michigan State University,
East Lansing, MI 48824, USA

Introduction

Bioelectronic interfaces that allow electrons to be exchanged between an enzyme and an underlying electrode have potential industrial applications, including biosensors [1, 2], biocatalytic reactors [3, 4], and biological fuel cells [5, 6]. Dehydrogenase enzymes are of particular interest for bioelectronic applications because they catalyze reactions that involve direct electron transfer. Alcohol dehydrogenases (ADHs) are zinc-containing enzymes that use either β-nicotinamide adenine dinucleotide (NAD^+) (EC 1.1.1.1), β-nicotinamide adenine dinucleotide phosphate ($NADP^+$) (EC 1.1.1.2), or both (EC 1.1.1.71) as a cofactor [7]. The ADHs are classified as either primary (1°) or secondary (2°) based on their efficiency in reacting either primary or secondary alcohols, respectively.

The $NADP^+$-dependent secondary ADH (2° ADH) from *Thermoanaerobacter ethanolicus* is a especially attractive enzyme for bioelectronic interface development because of its thermostability, ease of production, and ability to function in the presence of molecular oxygen [8, 9]. The cloning, purification, crystallization, and reaction properties for the 2° ADH have previously been reported [10–13]. Because NAD^+ is more stable and less expensive than $NADP^+$ [14], research is underway to engineer this enzyme so that it can use NAD^+ as a cofactor.

Dehydrogenase enzymes often require cofactor diffusion into the Rossmann fold, where electrons are transferred between the redox center of the protein and the cofactor. Thus, modification of the Rossmann fold via site-specific mutagenesis may alter the cofactor specificity. A triple mutation targeting the amino acids involved in cofactor binding has recently been used to transfer cofactor specificity in amphibian *Rana perezi* primary ADH (1° ADH) from $NADP^+$ to NAD^+ [15]. Peptide sequence alignments have shown that thermophilic and mesophilic 1° and 2° ADHs use a unique Cys–His–Asp (Cys^{37}–His^{59}–Asp^{150}) motif for catalytic metal ligation [16] and Gly^{198} as a residue responsible for cofactor binding [17]. Thus, the Cys^{37}, His^{59}, Asp^{150} and Gly^{198} have been targets for enzyme mutagenesis [17]. The replacement of Gly^{198} with Asp resulted in a threefold lower K_m(app) toward NAD^+ and a fivefold higher 2-propanol oxidation rate with NAD^+ compared with the wild type, indicating a partial shift in cofactor specificity from $NADP^+$ to NAD^+ [17]. However, Kleifeld and coworkers [18] found that Tyr^{267}, Tyr^{218}, Met^{285}, Arg^{200}, and His^{42} residues affect the rotation of the side chains of the cofactor in the Rossmann fold of *Thermoanaerobacter brockii*. Zeikus *et al*. (personal communication) have shown that the amino acid sequences for *T. ethanolicus* and *T. brockii* are the same, suggesting that the Tyr^{218} would be an amino acid on which to focus in the continued pursuit of an NAD^+-dependent 2° ADH.

Ideally, mutant dehydrogenase enzymes should not only have a desirable profile of cofactor and product specificities but they should also function effectively when incorporated into the bioelectronic interfaces suitable for industrial applications. The development of such interfaces has been hampered by challenges associated with regenerating the enzyme's cofactor in situ [19–21]. Methods have been developed to immobilize mediators, cofactors, and dehydrogenase enzymes at the electrode surface including the use of diffusional electron mediators [22], the immobilization of the enzymes in conductive polymers [23, 24], and the construction of a redox relay which conducts electrons between the enzyme and electrode [14, 25]. However, these electrodes result in the binding of the enzyme to the surface in a random orientation, resulting in inefficient electrical communication [26, 27]. To overcome this problem, Zayats et al. [27, 28] developed a linear molecular chain consisting of the electrode, mediator, cofactor, and enzyme. However, this approach requires the use of an electron mediator that forms two

bonds: one with the surface, and the other with the cofactor. We recently developed an electron-transfer scaffold using a heterotrifunctional linking molecule (e.g., cysteine, CYS) [29]. The electron mediator and cofactor were bound to opposite branches of the linking molecule, allowing greater flexibility in scaffold formation and permitting the use of electron mediators having a single reactive group.

This paper describes the site-directed mutagenesis of *T. ethanolicus* 2° ADH to replace the Tyr^{218} with Phe, and this work also describes the characterization of the resulting mutant enzyme (denoted Y218F 2° ADH). The K_m(app) and V_{max} values of the mutant and wild-type enzymes were measured. The performance of the mutant enzyme immobilized in a bioelectronic interface was also characterized using cyclic voltammetry, chronoamperometry, constant potential amperometry, gas chromatography, mass spectroscopy, and electrochemical impedance spectroscopy.

Materials and Methods

Chemicals and Reagents

A kanamycin-resistance GenBlock DNA cartridge used in the construction of the expression vector was purchased from GE Healthcare (Pittsfield, MA, USA) [30]. DNA for sequencing was isolated using a Wizard miniprep kit (Promega, Madison, WI, USA). PCR products were cloned using a TOPO TA PCR product cloning kit (Invitrogen, Carlsbad, CA, USA). Excised DNA from agarose gels was purified using a QIAEX II Gel extraction kit (Qiagen, Valencia, CA, USA). Tryptone, yeast extract, dithiothreitol (DTT), isopropyl-beta-D-thiogalactopyranoside (IPTG), and 5′-bromo-4-chloro-3-indolyl-beta-D-galactopyranoside (X-gal) were purchased from Fisher Scientific (Pittsburgh, PA, USA). All other chemicals, including NAD^+ and $NADP^+$, CYS, toluidine blue O (TBO), 3-carboxyphenyl boronic acid (CBA), 1-ethyl-3-(3-dimethylaminopropyl) carbodiimide (EDC), *N*-hydroxysuccinimide (NHS), glutaric dialdehyde (25% in water), 2-propanol, ammonium sulfate, sodium phosphate monobasic, and sodium phosphate dibasic, were purchased from Sigma-Aldrich (St. Louis, MO, USA). Ultrapure water (18.2 MΩ) was supplied by a Barnstead Nanopure-UV four-stage purifier (Barnstead International, Dubuque, IA, USA).

Mutagenesis

All DNA manipulations were done using the established protocols [31, 32]. A point mutation was introduced into the *T. ethanolicus* 39E *adhB* gene by PCR-based site-directed mutagenesis [31]. An oligonucleotide primer (P1) complementary to the noncoding strand was synthesized, including a *Kpn*I restriction site, the native *adhB* ribosome assembly site, and the *adhB* translation initiation codon. A second oligonucleotide primer (P2) was designed to include the complement to the *adhB* termination codon and an *Apa*I restriction site. The complementary 25–45 base oligonucleotide primers containing the mutant bases (Y218F: coding strand (P3) 5′-GATATTGTAAACTTTAAAGATGGTCC-3′, and the noncoding strand (P4) 5′-GGACCATCTTTAAAGTTTACAATATC-3′) were used in conjunction with the primers previously described to mutate and amplify the N-terminal (using primers P1 and P4) and C-terminal segments (P2 and P3) of the *adhB* gene separately. The two amplified segments were combined as a template in a final PCR

reaction, using primers P1 and P2, to achieve the whole mutated *adhB* gene. The mutated *adhB* gene was cloned into a pCR 2.1-TOPO vector. The plasmid was then transformed into the *Escherichia coli* TOP 10 and grown on Luria–Bertani (LB) media (10 g L^{-1} tryptone, 5 g L^{-1} yeast extract, and 5 g L^{-1} NaCl) with 1.2 and 0.5 mg mL^{-1} IPTG and X-gal, respectively. The correct clone was expressed in pBluescriptII KS(+) containing a kanamycin-resistance cartridge introduced in the *Eco*RI site. The Michigan State University Research Technology Support Facility performed oligonucleotide synthesis and DNA sequence analysis.

Media and Strains

E. coli (DH5α pADH B1M1-kan and DH5α pADH Y218F-kan) cultures containing the recombinant plasmids for 2° ADH or the mutant Y218F 2° ADH, respectively, were grown in a 10-L fermentor (Bioflo 3000, New Brunswick Scientific, Edison, NJ, USA) in a rich complex medium (20 g L^{-1} tryptone, 10 g L^{-1} yeast extract, and 5 g L^{-1} NaCl) under constant stirring at 37°C in the presence of 25 μg mL^{-1} kanamycin and 100 μg mL^{-1} ampicillin.

Enzyme Purification

The recombinant wild-type and mutant 2° ADH enzymes were purified aerobically from *E. coli* (DH5α pADH B1M1-kan and DH5α pADH Y218F-kan, respectively). After cell recovery via centrifugation, the pelleted cells were resuspended (0.5 g wet weight/ml) in buffer A (50 mM Tris/HCl, pH 8.0, 5 mM DTT, and 10 μM $ZnCl_2$) containing 3 μg mL^{-1} lysozyme, incubated at 37°C for 30 min, and French pressed under 15,000 psi pressure. The cell lysate was treated with DNAse I and centrifuged for 30 min at 15,000×*g* to obtain the initial cell extract. The clarified lysate was incubated at 85°C for 15 min, cooled on ice for 30 min, and centrifuged for 30 min at 15,000×*g*. $(NH_4)_2SO_4$ was added to the protein mixture to give a concentration of 17.4 g L^{-1} (50% saturation) and stirred at 4°C for 30 min to precipitate unwanted soluble protein. The mixture was centrifuged at 15,000×*g* for 30 min, and the supernatant was removed. To precipitate the enzyme, an additional 7.0 g L^{-1} of $(NH_4)_2SO_4$ was added to the supernatant to achieve 70% saturation, and the solution was continuously stirred at 4°C for 30 min. The resulting suspension was centrifuged at 15,000×*g* for 30 min, and the pellet was dissolved in buffer A. The enzyme solution was then dialyzed against buffer A for 24 h at 4°C, changing the buffer every 8 h. The enzyme was purified using a DEAE-Sepharose fast-flow anion exchange chromatography column (column bed 2.5× 17 cm). Protein adsorbed to the column was eluted using a linearly increasing potassium chloride gradient (0.0–0.3 M) in buffer A. The eluent was collected using a fraction collector, and the protein solution was concentrated by ultrafiltration with a 30-kDa YM-30 ultrafiltration membrane (Millipore Corporation, Billerica, MA, USA) and stored in sealed plastic tubes at −80°C.

Enzyme Kinetics

The assay used for thermostable 2° ADH activity measures $NADP^+$ reduction during the enzymatic oxidation of 2-propanol at 60°C [33]. The enzyme was incubated at 55°C for 15 min before determining the activity. The pH of Tris buffer was adjusted to be 8.0 at 60°C using a thermal correction factor of −0.031 ΔpH/°C. Assays to determine K_m(app) and V_{max}(app) for $NADP^+$ were conducted at 60°C using a 2-propanol concentration 20 times the K_m(app) value. The activity of 2° ADH was determined as a function of the cofactor concentration using a spectrophotometer at a wavelength of 340 nm. Kinetic parameters were

calculated from nonlinear best fits of the activity data to the Michaelis–Menten equation using Origin 7.5 (OriginLab, Northampton, MA, USA) [34]. Protein concentrations were determined using the modified Bradford assay.

Bioelectronic Interface Fabrication

Gold electrodes (circular electrodes with a radius of 0.23 cm; roughness factor approximately 1.2) were cleaned by immersion in piranha solution (seven parts by volume concentrated H_2SO_4 and three parts 30% aqueous H_2O_2). The electrodes were then rinsed with deionized water, dried under nitrogen, and stored in 0.1 M phosphate buffer solution (PBS) pH 7.4. The electrodes were treated with a Harrick plasma cleaner (Harrick Scientific Corporation, Broading Ossining, NY, USA) for 1 min under 50 sccm flow of oxygen at a pressure of 0.15 Torr. The electrodes were then rinsed with deionized water for 10 min.

The clean gold electrodes were soaked in a 0.1-M aqueous solution of CYS for 1 h at room temperature and thoroughly rinsed with water to remove weakly adsorbed CYS. The CYS-modified gold electrodes were incubated for 2 h in PBS containing 1 mM TBO, 10 mM NHS, and 5 mM EDC to covalently link TBO to the CYS monolayer (CYS–TBO). A 5-mM CBA solution was activated at room temperature with 10 mM NHS and 5 mM EDC in PBS for 2 h. The activated CBA was then reacted with the CYS–TBO-modified electrodes for 1 h at room temperature [28] and rinsed with deionized water to remove weakly adsorbed CBA. The resulting CYS–TBO–CBA-modified electrodes were reacted with a 1-mM solution of either NAD^+ or $NADP^+$ in PBS for 1 h and then washed with water to remove any weakly bound cofactor. These modifications resulted in a gold electrode functionalized with CYS, TBO, and either NAD^+ or $NADP^+$. The CYS–TBO–$NADP^+$-functionalized gold electrodes were reacted with a 4.4-mg mL^{-1} solution of wild-type 2° ADH in PBS for 1 h and then cross-linked with 25% (*v*/*v*) glutaric acid in water for 20 min. The CYS–TBO–NAD^+-functionalized electrodes were reacted with 3.7 mg mL^{-1} Y218F 2° ADH in PBS for 1 h and cross-linked with 25% (*v*/*v*) glutaric acid in water for 20 min. The resulting bioelectronic interfaces were rinsed with water and used for the biocatalytic oxidation of 2-propanol.

Electrochemical Measurements

A conventional three-electrode cell consisting of an enzyme-modified gold working electrode, a platinum auxiliary electrode, and a silver/silver chloride (Ag/AgCl) reference electrode was used for electrochemical measurements. All potentials are reported with respect to a standard Ag/AgCl reference electrode. Electrochemical measurements were made in a grounded Faraday cage (Bioanalytical Systems (BAS), West Lafayette, IN, USA). Cyclic voltammetry, constant potential amperometry, and chronoamperometry were performed using a potentiostat/galvanostat (BAS, CV-50W) connected to a computer running BAS CV-50W (Version 2.3) software. Chronoamperometric and constant potential amperometric experiments were conducted by stepping the potential of the working electrode from −200 to 400 mV and measuring the current response. Cyclic voltammetric experiments were conducted by sweeping the potential of the working electrode from −200 to 400 mV at a scan rate of 100 mV s^{-1}, causing analyte in the vicinity of the electrode to be oxidized in the forward cycle and reduced in the reverse cycle. Impedance spectroscopy measurements were performed using a potentiostat/frequency response detector (CH Instruments, Model 650 A, Austin, TX, USA) connected to a computer running an Electrochemical Bench software (Solartron Analytical, Farnborough, Hampshire, United

Kingdom). Impedance measurements were performed in the frequency range from 10^{-1} to 10^{4} Hz at an open-circuit potential of 212 mV. A Randles' equivalent-circuit model was fit to the data using a Z-view software (Scribner Associates, Inc., Version 2.1b, Southern Pines, NC, USA) [35, 36].

Measurement of Catalytic Activity

To confirm catalytic activity of the mutant enzyme, a Y218F 2° ADH-modified electrode maintained at a constant potential of 400 mV was contacted with 10 mL of 25 mM 2-propanol under constant stirring at room temperature for 45 min. At 400 mV, nicotinamide adenine dinucleotide phosphate (NADPH) is oxidized in the presence of TBO [29]. Liquid samples were analyzed for 2-propanol and acetone using a JEOL AX505H double-focusing mass spectrometer (MS) (Japan Electronic Optics Laboratories, Peabody, MA, USA) equipped with a Hewlett-Packard 6890J gas chromatograph (GC) (Palo Alto, CA, USA) and a 30 DB1 fused silica column. The oven temperature was held at 40°C for 5 min and then ramped at 10°C min^{-1} to 280°C.

Results and Discussion

Cofactor Specificity

Kinetic parameters for the wild-type and mutant 2° ADH are given in Table 1. The wild-type enzyme exhibited a 150-fold lower K_m(app) for $NADP^+$ than for NAD^+ and a V_{max}(app) that was 16.5 times greater for $NADP^+$ than for NAD^+. When NAD^+ was the cofactor, the mutant exhibited a 2.7-fold lower K_m(app) and 5.5-fold higher V_{max}(app) than the wild type. When $NADP^+$ was used as the cofactor, the mutant exhibited a 200-fold greater K_m(app) and a threefold lower V_{max}(app) than the wild type. These trends are consistent with the results of Kleifeld and coworkers [18].

Electrochemical Measurements

Figure 1 shows the cyclic voltammograms obtained at a constant 2-propanol concentration of 2.5×10^{-2} M for different times of wild-type 2° ADH adsorption on the CYS–TBO–$NADP^+$-modified electrode. The anodic current increased with time and reached a saturation value after 1 h. Figure 1, inset, shows the peak anodic current as a function of adsorption time. The pseudo first-order adsorption time constant ($\tau_{wt\text{-}NADP}$) derived from the data was 18 min. When the experiment was repeated for the adsorption of the wild-type 2° ADH onto the CYS–TBO–NAD^+-modified electrode, the anodic current reached a

Table 1 Apparent K_m and V_{max} values for the wild type and Y218F mutant.

Enzyme	$NADP^+$		NAD^+	
	V_{max}(app) (U mg^{-1})	K_m(app) (mM)	V_{max}(app) (U mg^{-1})	K_m(app) (mM)
Wild type	69	0.017	4.2	2.5
Y218F mutant	21	3.4	23	0.93

2-Propanol was used as the cosubstrate in all cases. The values of K_m and V_{max} for the wild-type 2° ADH and the Y218F 2° ADH mutant were determined for each cofactor.

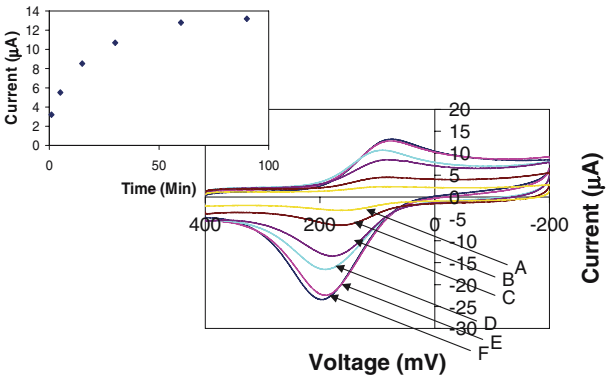

Fig. 1 Cyclic voltammograms of the TBO–CBA–$NADP^+$-functionalized Au electrode after various times of wild-type 2° ADH reconstitution: **A** 1 min, **B** 5 min, **C** 15 min, **D** 30 min, **E** 60 min, and **F** 90 min. The data were recorded in room-temperature PBS, containing 3.0×10^{-2} M 2-propanol, at a potential scan rate of 100 mV s^{-1}. *Inset* Peak electrocatalytic current at various time intervals

saturated value after 3 h with a pseudo first-order time constant ($\tau_{wt\text{-}NAD}$) of 45 min (data not shown). The decrease in the pseudo first-order rate coefficient suggests that the wild-type 2° ADH has a greater affinity for $NADP^+$ than NAD^+. The pseudo first-order time constant ($\tau_{Y218F\text{-}NAD}$) for the Y218F 2° ADH on the CYS–TBO–NAD^+-modified electrode was determined to be 35 min (data not shown). This increase in the pseudo first-order rate coefficient suggests that Y218F 2° ADH has a greater affinity for NAD^+ than the wild-type 2° ADH.

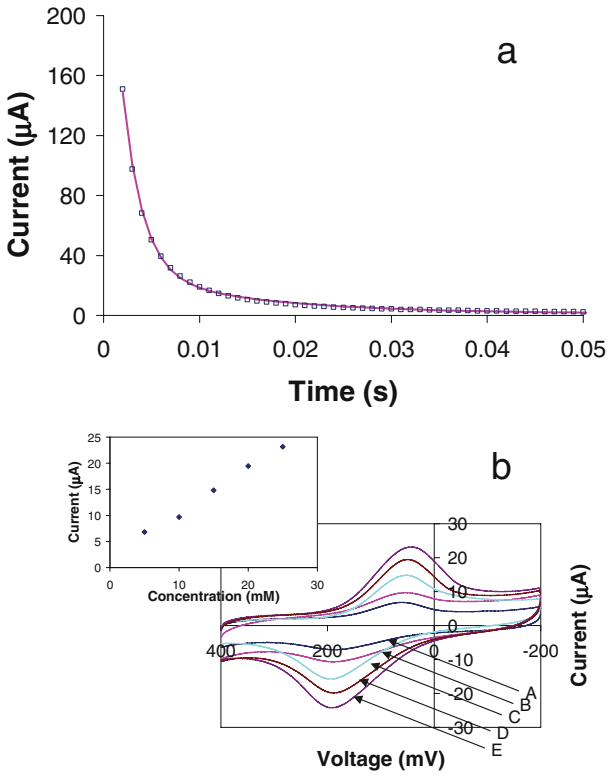

Fig. 2 **a** Chronoamperometric current transient after a potential step from $E_{initial}$=−200 mV to E_{final}=400 mV for the wild-type 2° ADH associated with the CYS–TBO–CBA–$NADP^+$-functionalized electrode. **b** Cyclic voltammograms for the CYS–TBO–$NADP^+$-functionalized Au electrode containing wild-type 2° ADH in the presence of different concentrations of 2-propanol: *A* 5.0×10^{-3} M, *B* 1.0×10^{-2} M, *C* 1.5×10^{-2} M, *D* 2.0×10^{-2} M, and *E* 2.5×10^{-2} M . The data were recorded in room-temperature PBS at a potential scan rate of 100 mV s^{-1}. *Inset* Peak electrocatalytic current at various 2-propanol concentrations

Figure 2a shows the chronoamperometric current response for the CYS–TBO–$NADP^+$ 2° ADH-modified electrode in the presence of 2-propanol after a potential step from −200 to 400 mV. The rate of change in current depends on the spatial orientation of the components comprising the interface. Redox components with multiple binding modes have been shown to exhibit a specific rate constant for each binding mode [27]. Because $NADP^+$ has a single *cis*-diol moiety capable of forming a boronic acid linkage (Scheme 1), a single exponential decay model, Eq. 1, was fit to the data [37]:

$$I = k_{et} Q \exp(-k_{et} t) \tag{1}$$

where k_{et} is the electron-transfer rate constant, and Q is the amount of charge transferred after the potential step. Fitting Eq. 1 to the chronoamperometric data using Origin 7.5 gives a k_{et} value of 480 s^{-1} for the 2° ADH-modified electrodes. The corresponding value of the surface coverage (Γ) was calculated using Eq. 2 [27]:

$$\Gamma = \frac{Q}{nFA} \tag{2}$$

where F is the Faraday's constant, A is the electrode area (0.16 cm^2), and n is the number of electrons transferred (n=2) in the reaction. The resulting Γ value of 2.1×10^{-11} mol cm^{-2} represents the surface density of functional bioelectronic complexes being able to achieve multistep electron transfer between the enzyme, cofactor, mediator, and electrode.

Figure 2b shows the cyclic voltammograms of the reconstituted enzyme electrodes at different concentrations of 2-propanol. The anodic wave began at the oxidation potential of the bound TBO (200 mV), suggesting that TBO mediates the electron transfer between the bound cofactor and the electrode [27]. The peak anodic current varied linearly with 2-propanol

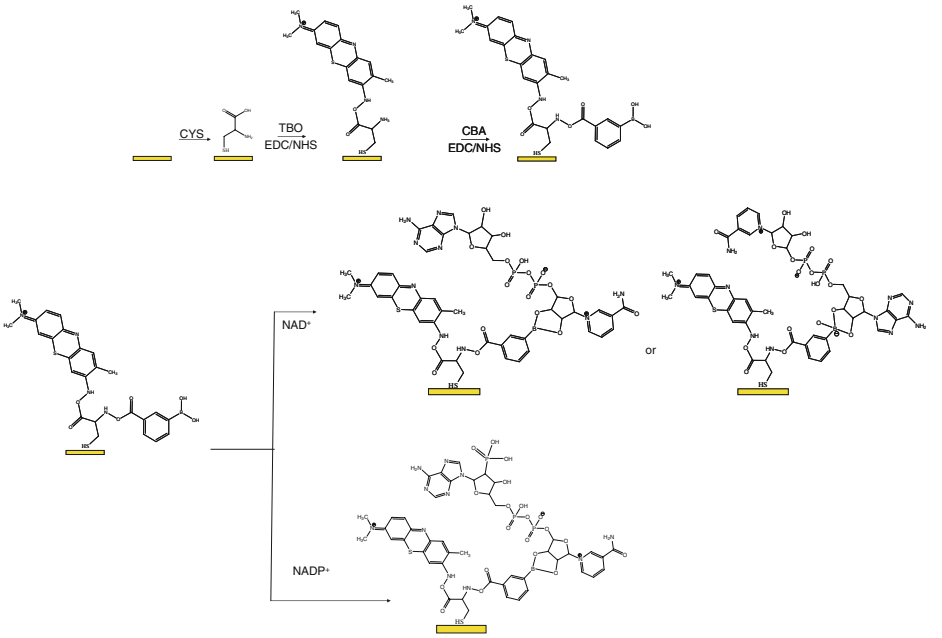

Scheme 1 Molecular architecture of the bioelectronic interface used to couple the electron mediator and cofactor to a cysteine-functionalized gold electrode

concentration, Fig. 2b inset, indicating that interface can function as a 2-propanol biosensor. The slope of this calibration curve, 0.85 μA mM^{-1}, is a measure of the biosensor's sensitivity. At higher concentrations, the anodic current reached a saturation value ($I_{cat}^{sat} = 23$ μA). Using this value, along with the surface coverage (Γ=2.1×10^{-11} mol cm^{-2}), the electrode area, and the number of electrons transferred during oxidation, the maximum turnover rate (TR_{max}) was calculated to be 32 s^{-1} using Eq. 3, where I_0 is the background current.

$$TR_{max} = \frac{I_{cat}^{sat} - I_0}{(Fn\Gamma A)} \tag{3}$$

This value represents the number of molecules of 2-propanol oxidized per 2° ADH molecule per second. The CYS–$NADP^+$–wild-type 2° ADH-integrated electrodes exhibited 2% degradation in activity after continuous operation for 24 h at room temperature. When stored in 0.1 M borate buffer (pH 7.5) solution at room temperature for 2 weeks, the electrodes exhibited no measurable loss in performance.

Figure 3a shows the chronoamperometric current for the CYS–TBO–NAD^+–wild-type 2° ADH-modified electrode after a potential step from −200 to 400 mV. While $NADP^+$ has a single *cis*-diol group that can bind to the boronic acid, NAD^+ has two; thus, two binding modes are feasible, as shown in Scheme 1. For this reason, a biexponential decay model (Eq. 4) was used to analyze the data [27]:

$$I = k'_{et}Q' \exp(-k'_{et}t) + k''_{et}Q'' \exp\left(-k''_{et}t\right) \tag{4}$$

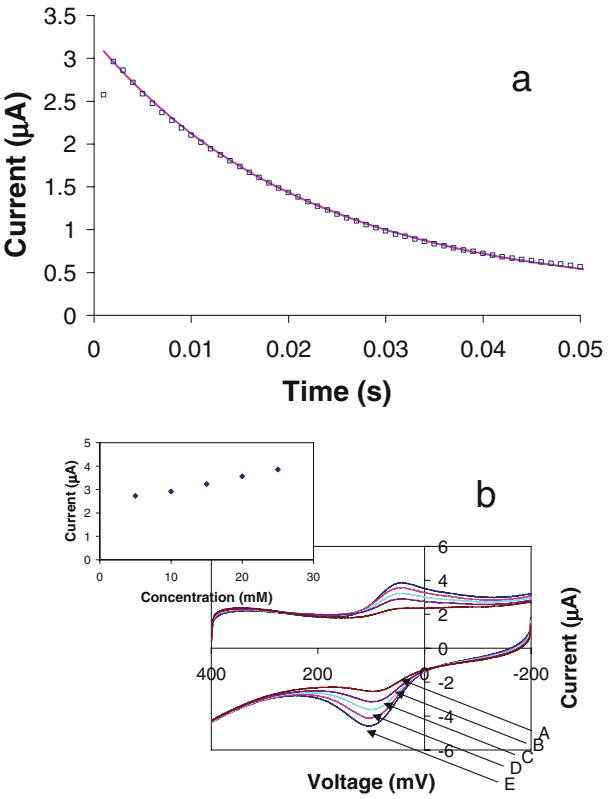

Fig. 3 **a** Chronoamperometric current transient after a potential step from $E_{initial}$=−200 mV to E_{final}=400 mV for the wild-type 2° ADH associated with the CYS–TBO–CBA–NAD^+-functionalized electrode. **b** Cyclic voltammograms for the CYS–TBO–NAD^+-functionalized Au electrode containing wild-type 2° ADH in the presence of different concentrations of 2-propanol: *A* 5.0×10^{-3} M, *B* 1.0×10^{-2} M, *C* 1.5×10^{-2} M, *D* 2.0×10^{-2} M, and *E* 2.5×10^{-2} M. The data were recorded in room-temperature PBS at a potential scan rate of 100 mV s^{-1}. *Inset* Peak electrocatalytic current at various 2-propanol concentrations

where k'_{et} and k''_{et} are the electron-transfer rate constants for the two binding modes, and Q' and Q'' are the corresponding amounts of charge transferred by each binding mode. Fitting Eq. 4 to the chronoamperometric data, using Origin 7.5, gives k'_{et} and k''_{et} values of 45 and 1.4 s^{-1}, respectively. The resulting surface coverages for the two binding modes were determined to be 2.2×10^{-12} and 1.5×10^{-11} mol cm^{-2}, giving a total surface coverage of 1.7×10^{-11} mol cm^{-2}.

Figure 3b shows the cyclic voltammograms for the biocatalytic oxidation of 2-propanol at the CYS–TBO–NAD^+–wild-type 2° ADH-integrated electrode. The plot of the peak current vs 2-propanol concentration, shown in Fig. 3b (inset), increases linearly with 2-propanol concentration and has a slope of 0.07 μA mM^{-1}. At higher concentrations, the anodic current reached a saturation value (4.0 μA). The value was used, along with the surface coverage (1.7×10^{-11} mol cm^{-2}), the electrode area, and the number of electrons transferred during oxidation to calculate a TR_{max} of 3.8 s^{-1} using Eq. 3. Thus, the turnover rate of the CYS–TBO–NAD^+–wild-type 2° ADH-integrated electrode is one-tenth that of CYS–TBO–$NADP^+$–wild-type 2° ADH-integrated electrode, confirming that the wild-type 2° ADH has increased activity in the presence of $NADP^+$.

Figure 4a shows the chronoamperometric current for the CYS–TBO–NAD^+–Y218F 2° ADH-modified electrode after a potential step from −200 to 400 mV. The k'_{et} and k''_{et} values were determined to be 210 and 46 s^{-1}, respectively. The increase in the electron-transfer coefficients compared to the CYS–TBO–NAD^+–wild-type 2° ADH-modified interface suggests that the mutant enzyme exchanges electrons with NAD+ more efficiently than does the wild type. The resulting surface coverages for the two binding

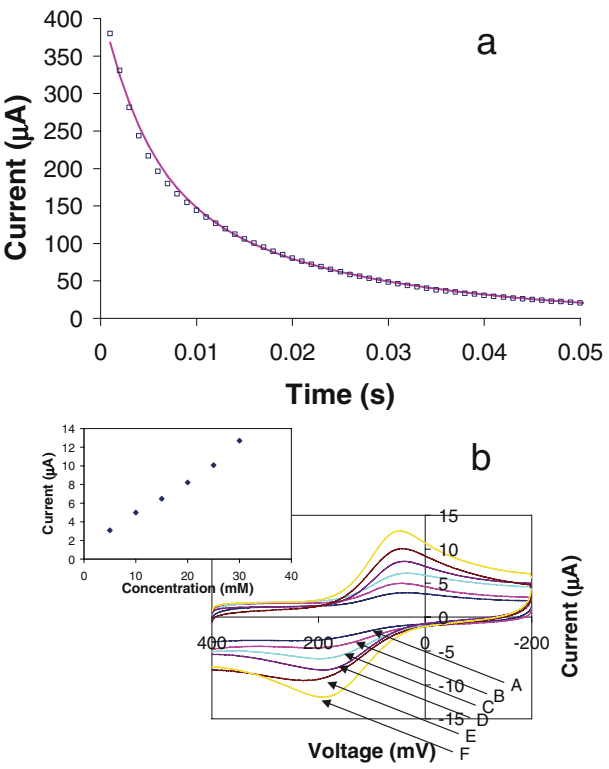

Fig. 4 **a** Chronoamperometric current transient after a potential step from $E_{initial}$=−200 mV to E_{final}=400 mV for the Y218F 2° ADH associated with the CYS–TBO–CBA–NAD^+-functionalized electrode. **b** Cyclic voltammograms of the CYS–TBO–NAD^+-functionalized Au electrode adsorbed Y218F 2° ADH in the presence of different concentrations of 2-propanol: *A* 5.0×10^{-3} M, *B* 1.0×10^{-2} M, *C* 1.5×10^{-2} M, *D* 2.0×10^{-2} M, and *F* 3.0×10^{-2} M. The measurements were performed in PBS at a scan rate of 100 mV s^{-1}. *Inset* Peak electrocatalytic current at various 2-propanol concentrations

modes were determined to be 3.6×10^{-12} and 1.3×10^{-11} mol cm^{-2}, respectively, for a total surface coverage of 1.7×10^{-11} mol cm^{-2}.

Figure 4b shows the cyclic voltammograms for the biocatalytic oxidation of 2-propanol at the CYS–TBO–NAD$^+$–Y218F 2° ADH-integrated electrode. The plot of the peak current vs 2-propanol concentration increases linearly with a slope of 0.37 μA mM^{-1}. At higher concentrations, the anodic current reaches saturation at a current of 13 μA. The saturation current, the surface coverage (1.7×10^{-11} mol cm^{-2}), the electrode area, and the number of electrons transferred during oxidation were used to calculate a TR_{max} of 23 s^{-1} using Eq. 3. Thus, the mutant exhibits a turnover rate four times higher than the wild-type enzyme. Figure 5a shows the chronoamperometric step responses of the CYS–TBO–NAD$^+$–Y218F 2° ADH-modified electrode after the successive addition of 500 μM acetone to PBS, pH 7.4, under constant stirring at a constant potential of −200 mV. Figure 5b shows that the anodic current increases linearly with the concentration between 500 μM and 3 mM, with a sensitivity and a limit of detection of 0.9 μA mM^{-1} and 50 μM, respectively. No measurable loss of performance was observed for this interface upon storage in 0.1 M borate buffer (pH 7.0) at room temperature for 2 weeks.

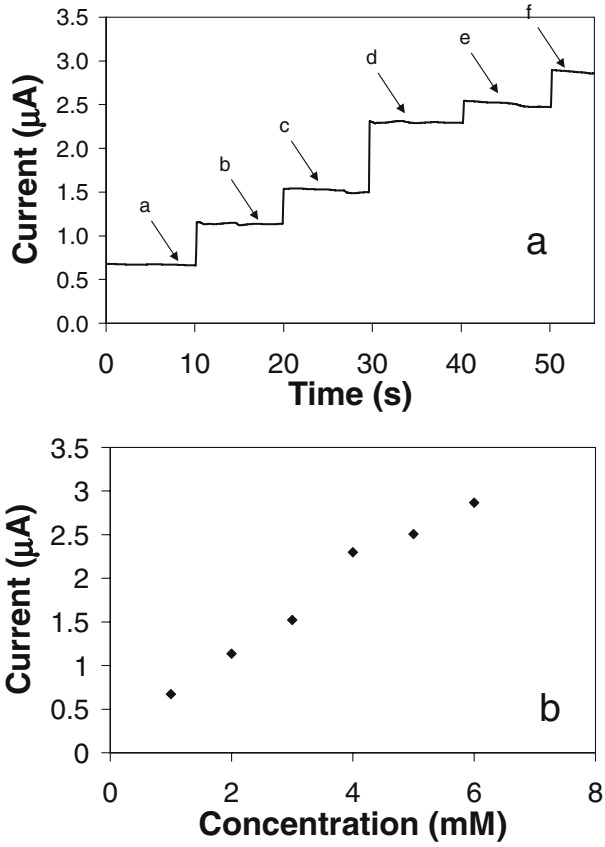

Fig. 5 **a** Constant potential amperometric measurements for the TBO–CBA–NAD$^+$ electrode containing Y218F 2° ADH in the presence of different concentrations of acetone: *a* 1.0×10^{-3} M, *b* 2.0×10^{-3} M, *c* 3.0×10^{-3} M, *d* 4.0×10^{-3} M, *e* 5.0×10^{-3} M, *f* 6.0×10^{-3} M. **b** Calibration curve consisting of bioelectronic current plotted vs acetone concentration

Biocatalytic Reactor

Gas chromatography–mass spectrometry was used to confirm that a bioelectronic interface containing the mutant enzyme could oxidize 2-propanol to acetone. The GC trace for the reactant revealed a single peak (Fig. 6a), which MS analysis confirmed to be due to 2-propanol. After the 45-min reaction period, the GC trace indicated two peaks (Fig. 6b), which MS confirmed were due to 2-propanol (Fig. 6c) and acetone (Fig. 6c). Because 2-propanol and acetone have similar molecular structures, the peak areas can be directly compared to estimate the relative concentrations. Using this approach, the final concentration of acetone (C_{Ac}) was estimated to be about 2 mM. This value was then used to calculate the average number of times that each NADP(H) molecule was electrically turned over (T_e) during the experiment using Eq. 5:

$$T_e = \frac{C_{Ac} V}{\Gamma A} \tag{5}$$

where V is the liquid volume. The calculated T_e value of 6.7×10^4, together with the previously mentioned stability results, suggests that the bioelectronic interface containing the

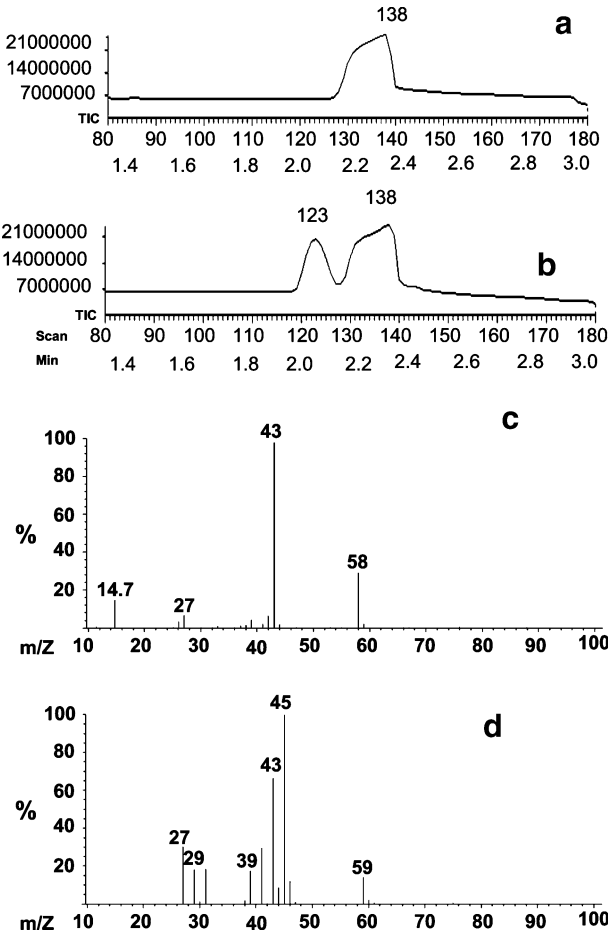

Fig. 6 GC–MS analysis of the reaction solutions before and after the 45-min reaction period: **a** GC spectrum of the initial reaction mixture. **b** GC spectrum of the product after a 45-min reaction period. **c** Mass spectrum of the GC peak eluting at a retention time of 2.1 min. **d** Mass spectrum of the GC peak eluting at a retention time of 2.3 min. The spectra in curves **(c)** and **(d)** correspond to 2-propanol and acetone, respectively

mutant enzyme has sufficient stability to be evaluated for commercial bioreactor and biosensor applications.

Conclusions

This study demonstrated site-directed mutagenesis of Tyr^{218} to Phe in thermophilic *T. ethanolicus* 2° ADH. Using NAD^+ as the cofactor, the Y218F mutant enzyme exhibited a 5.5-fold higher V_{max} and a 2.7-fold lower K_m for NAD^+ than the wild type. When immobilized on the CYS–TBO–NAD^+-modified interface, the electron transfer coefficients for the Y218F mutant enzyme were 210 and 46 s^{-1} compared to 45 and 1.4 s^{-1} for the wild type. The NAD^+-containing bioelectronic interface containing the Y218F mutant exhibited a sensitivity of 0.37 μA mM^{-1} compared to 0.07 μA mM^{-1} for the wild type. The electrocatalytic activity of the Y218F 2° ADH measured using GC–MS indicated that the NAD^+ was recycled 6.7×10^4 times during the course of a 45-min experiment. Collectively, these results provide strong evidence that the Tyr^{218} to Phe mutation adjusted the 2° ADH cofactor specificity toward NAD^+.

The ability to use an NAD^+-dependent 2° ADH offers potential for commercial biosensors and biocatalytic reactors having increased stability and reduced costs.

Acknowledgments The authors would like to thank the Michigan Technology Tri-Corridor (MTTC) program of the Michigan Economic Development Corporation (MEDC) and the IRGP programs at Michigan State University (MSU) for funding this work. Analytical support provided by the analytical chemistry facility in the MSU Department of Chemistry is also gratefully acknowledged.

References

1. Armstrong, F. A., Heering, H. A., & Hirst, J. (1997). Reactions of complex metalloproteins studied by protein-film voltammetry. *Chemical Society Reviews, 26*(3), 169–179.
2. Halbhuber, Z., Petrmichlova, Z., Alexciev, K., Thulin, E., & Stys, D. (2003). Overexpression and purification of recombinant membrane PsbH protein in Escherichia coli. *Protein Expression and Purification, 32*(1), 18–27.
3. Park, D. H., Laivenieks, M., Guettler, M. V., Jain, M. K., & Zeikus, J. G. (1999). Microbial utilization of electrically reduced neutral red as the sole electron donor for growth and metabolite production. *Applied and Environmental Microbiology, 65*(7), 2912–2917.
4. Park, D. H., & Zeikus, J. G. (1999). Utilization of electrically reduced neutral red by Actinobacillus succinogenes: Physiological function of neutral red in membrane-driven fumarate reduction and energy conservation. *Journal of Bacteriology, 181*(8), 2403–2410.
5. Chen, T., Barton, S. C., Binyamin, G., Gao, Z. Q., Zhang, Y. C., Kim, H. H., et al. (2001). A miniature biofuel cell. *Journal of the American Chemical Society, 123*(35), 8630–8631.
6. Tsujimura, S., Fujita, M., Tatsumi, H., Kano, K., & Ikeda, T. (2001). Bioelectrocatalysis-based dihydrogen/dioxygen fuel cell operating at physiological pH. *Physical Chemistry Chemical Physics, 3*(7), 1331–1335.
7. Jornvall, H., Eklund, H., & Branden, C. I. (1978). Subunit conformation of yeast alcohol-dehydrogenase. *Journal of Biological Chemistry, 253*(23), 8414–8419.
8. Keinan, E., Hafeli, E. K., Seth, K. K., & Lamed, R. (1986). Thermostable enzymes in organic-synthesis 2. Asymmetric reduction of ketones with alcohol-dehydrogenase from Thermoanaerobium-Brockii. *Journal of the American Chemical Society, 108*(1), 162–169.
9. Keinan, E., Seth, K. K., & Lamed, R. (1987). Synthetic applications of alcohol-dehydrogenase from Thermoanaerobium-Brockii. *Annals of the New York Academy of Sciences, 501*, 130–149.
10. Heiss, C., Laivenieks, M., Zeikus, J. G., & Phillips, R. S. (2001). Mutation of cysteine-295 to alanine in secondary alcohol dehydrogenase from Thermoanaerobacter ethanolicus affects the enantioselectivity and substrate specificity of ketone reductions. *Bioorganic & Medicinal Chemistry, 9*(7), 1659–1666.

11. Tripp, A. E., Burdette, D. S., Zeikus, J. G., & Phillips, R. S. (1998). Mutation of serine-39 to threonine in thermostable secondary alcohol dehydrogenase from Thermoanaerobacter ethanolicus changes enantiospecificity. *Journal of the American Chemical Society, 120*(21), 5137–5141.
12. Kosjek, B., Stampfer, W., Pogorevc, M., Goessler, W., Faber, K., & Kroutil, W. (2004). Purification and characterization of a chemotolerant alcohol dehydrogenase applicable to coupled redox reactions. *Biotechnology and Bioengineering, 86*(1), 55–62.
13. Peretz, M., Bogin, O., TelOr, S., Cohen, A., Li, G. S., Chen, J. S., et al. (1997). Molecular cloning, nucleotide sequencing, and expression of genes encoding alcohol dehydrogenases from the thermophile Thermoanaerobacter brockii and the mesophile Clostridium beijerinckii. *Anaerobe, 3*(4), 259–270.
14. Schuhmann, W., Ohara, T. J., Schmidt, H. L., & Heller, A. (1991). Electron-transfer between glucose-oxidase and electrodes via redox mediators bound with flexible chains to the enzyme surface. *Journal of the American Chemical Society, 113*(4), 1394–1397.
15. Rosell, A., Valencia, E., Ochoa, W. F., Fita, I., Pares, X., & Farres, J. (2003). Complete reversal of coenzyme specificity by concerted mutation of three consecutive residues in alcohol dehydrogenase. *Journal of Biological Chemistry, 278*(42), 40573–40580.
16. Burdette, D. S., Vieille, C., & Zeikus, J. G. (1996). Cloning and expression of the gene encoding the Thermoanaerobacter ethanolicus 39E secondary-alcohol dehydrogenase and biochemical characterization of the enzyme. *Biochemical Journal, 316*, 115–122.
17. Burdette, D. S., Secundo, F., Phillips, R. S., Dong, J., Scott, R. A., & Zeikus, J. G. (1997). Biophysical and mutagenic analysis of Thermoanaerobacter ethanolicus secondary alcohol dehydrogenase activity and specificity. *Biochemical Journal, 326*, 717–724.
18. Kleifeld, O., Frenkel, A., Bogin, O., Eisenstein, M., Brumfeld, V., Burstein, Y., et al. (2000). Spectroscopic studies of inhibited alcohol dehydrogenase from Thermoanaerobacter brockii: Proposed structure for the catalytic intermediate state. *Biochemistry, 39*(26), 7702–7711.
19. Blaedel, W. J., & Jenkins, R. A. (1975). Study of electrochemical oxidation of reduced nicotinamide adenine-dinucleotide. *Analytical Chemistry, 47*(8), 1337–1343.
20. Prodromidis, M. I., & Karayannis, M. I. (2002). Enzyme based amperometric biosensors for food analysis. *Electroanalysis, 14*(4), 241–261.
21. Schmakel, C. O., Santhanam, K. S. V., & Elving, P. J. (1975). Nicotinamide adenine-dinucleotide (Nad+) and related compounds - electrochemical redox pattern and allied chemical behavior. *Journal of the American Chemical Society, 97*(18), 5083–5092.
22. Serban, S., & El Murr, N. (2004). Synergetic effect for NADH oxidation of ferrocene and zeolite in modified carbon paste electrodes - new approach of dehydrogenase based biosensors. *Biosensors & Bioelectronics, 20*(2), 161–166.
23. Emr, S. A., & Yacynych, A. M. (1995). Use of polymer-films in amperometric biosensors. *Electroanalysis, 7*(10), 913–923.
24. Heller, A. (1990). Electrical wiring of redox enzymes. *Accounts of Chemical Research, 23*(5), 128–134.
25. Degani, Y., & Heller, A. (1987). Direct electrical communication between chemically modified enzymes and metal-electrodes 1. Electron-transfer from glucose-oxidase to metal-electrodes via electron relays, bound covalently to the enzyme. *Journal of Physical Chemistry, 91*(6), 1285–1289.
26. Badia, A., Carlini, R., Fernandez, A., Battaglini, F., Mikkelsen, S. R., & English, A. M. (1993). Intramolecular electron-transfer rates in ferrocene-derivatized glucose-oxidase. *Journal of the American Chemical Society, 115*(16), 7053–7060.
27. Zayats, M., Katz, E., & Willner, I. (2002). Electrical contacting of flavoenzymes and NAD(P)(+)-dependent enzymes by reconstitution and affinity interactions on phenylboronic acid monolayers associated with Au-electrodes. *Journal of the American Chemical Society, 124*(49), 14724–14735.
28. Riklin, A., Katz, E., Willner, I., Stocker, A., & Buckmann, A. F. (1995). Improving enzyme-electrode contacts by redox modification of cofactors. *Nature, 376*(6542), 672–675.
29. Hassler, B. L., & Worden, R. M. (2006). Versatile bioelectronic interfaces based on heterotrifunctional linking molecules. *Biosensors & Bioelectronics, 21*(11), 2146–2154.
30. Oka, A., Sugisaki, H., & Takanami, M. (1981). Nucleotide-sequence of the Kanamycin Resistance Transposon Tn903. *Journal of Molecular Biology, 147*(2), 217–226.
31. Sambrook, J. M., Fritsch, E. F., & Maniatis, T. (1989). *Molecular cloning: A laboratory manual* (2nd edn.). Cold Springs Harbor, NY: Cold Springs Harbor Laboratory Press.
32. Ausubel, F. M., Brent, R., Kingston, R. E., Moore, D. D., Seidman, J. G., Smith, J. A., et al. (1993). *Current protocols in molecular biology.* New York, NY: Greene Publishing and Wiley-Interscience.
33. Burdette, D., & Zeikus, J. G. (1994). Purification of acetaldehyde dehydrogenase and alcohol dehydrogenases from Thermoanaerobacter-ethanolicus 39e and characterization of the secondary-alcohol dehydrogenase(2-Degrees Adh) as a bifunctional alcohol-dehydrogenase acetyl-Coa reductive thioesterase. *Biochemical Journal, 302*, 163–170.

34. Brooks, S. P. J. (1992). A simple computer-program with statistical tests for the analysis of enzyme-kinetics. *Biotechniques, 13*(6), 906–911.
35. Armstrong, R. D., Bell, M. F., & Metcalfe, A. A. (1977). Method for automatic impedance measurement and analysis. *Journal of Electroanalytical Chemistry, 77*(3), 287–298.
36. Mostany, J., & Scharifker, B. R. (1997). Impedance spectroscopy of undoped, doped and overoxidized polypyrrole films. *Synthetic Metals, 87*(3), 179–185.
37. Katz, E., & Willner, I. (1997). Kinetic separation of amperometric responses of composite redox-active monolayers assembled onto Au electrodes: Implications to the monolayers' structure and composition. *Langmuir, 13*(13), 3364–3373.